Human-Cable Collision Detection with a Cable-Driven Parallel Robot

Sophie Rousseau, Christine Chevallereau, Stéphane Caro

Human-Cable Collision Detection with a Cable-Driven Parallel Robot

Thomas Rousseau[1], Christine Chevallereau[2], Stéphane Caro[2,*]

Abstract

This paper deals with human-cable collision detection with a Cable-Driven Parallel Robot (CDPR) and a control strategy to safely release the tension in the cable in contact with a human operator. The main purpose of this work is to contribute to the development of safety solutions allowing collaborative work between human and robot with CDPRs in production tasks. Using a geometric model of cable deformations under an external collision, a direct relationship is established between the initial cable tension, the collision force and the increase in cable tension. This relationship is validated experimentally with an ad-hoc test bench. Collision force levels are set to admissible values in order to prevent harm for human operators. A collision detection is then implemented on the 8-cable suspended CDPR CRAFT prototype using this method, continuously comparing the cable tensions measured by sensors with admissible cable tension increases. Using these results, an approach aiming at releasing a collided cable so as to minimize risks for operators and the environment of the robot is proposed with an adaptive control scheme, based on a progressive cable tension management once a collision is detected. This cable tension management is simulated and represented in the null space of CDPR wrench matrix. Feasibility domain of this tension management and alternative solutions outside of it are also discussed. This work contributes to the safety of collaborative CDPRs by determining a direct relationship between collision force and cable tensions in the event of a collision and by introducing a collision detection method.

Keywords: Cable-Driven Parallel Robots, Cobotics, Collision, Safety

1. Introduction

The development of automation in the industry saw the increasing presence in workplaces of various industrial robot models, and starting from the last two decades, of cobots. Collaborative robotics are already used in the industry, for instance in automotive factories for several tasks [1]. Collaborative robotics aims at removing the fences around robots to allow them to cooperate with workers [2]. This enables a level of automation in tasks where a robot would lack the dexterity or the problem-solving ability of humans, while protecting the latter from dangerous or dull tasks which are generally responsible for workplace injuries such as musculoskeletal disorders [3]. But this also extends to robots operating in the same workspace as human operators, while not necessarily performing a common task [4]. One of the main preoccupations in cobotics is the safety of the workers co-acting or co-manipulating with cobots. Hence, an important part of the research related to this field is connected to safety functions, for instance developing collision avoidance [5], safety-rated monitored stop, speed monitoring or power and force limiting [6]. Collision detection approaches have been experimented for rigid-link collaborative robots in [7, 8].

However, these cobots usually have a small workspace. Hence, assembly applications in industrial sectors such as aeronautics or the construction industry, where large workspaces are required, especially for assembly tasks, are outside of the scope of conventional cobotic systems.

Conversely, Cable-Driven Parallel Robots (CDPRs) have the potential of offering larger workspaces, including in collaborative applications [9]. CDPRs form a particular class of parallel robots, using cables instead of rigid links. Their End-Effector (EE), also named mobile platform or simply platform, boards the payload that will perform the required tasks, moving inside the space within the frame defined as the workspace.

An example of CDPR dedicated to cobotics applications is shown Fig. 1. This prototype, named CRAFT, was designed by the LS2N laboratory in Nantes, France for the development of new robotic systems for agile operations in manufacturing facilities. The collision detection method proposed in this paper was validated experimentally on the CRAFT prototype.

Each cable has one end connected to this platform, while the other is coiled on a drum actuated by a motor fixed to the ground. Usually, pulleys are placed between the drum and the end point on the platform. These pulleys define the exit points of the cables and the cable length between them and the anchor points on the mobile platform is the controlled distance in order to command the robot pose (position + orientation).

CDPRs originated in the end of the 1980 decade, the NIST Robocrane being the first large prototype [10, 11]. These robots raised the interest of several industrial firms because of their ad-

*Corresponding author

Email addresses: thomas.rousseau@ls2n.fr (Thomas Rousseau), christine.chevallereau@ls2n.fr (Christine Chevallereau), stephane.caro@ls2n.fr (Stéphane Caro)

[1]Laboratoire des Sciences du Numérique de Nantes, 44321 Nantes, France and IRT Jules Verne, Bouguenais, 44340, France

[2]Laboratoire des Sciences du Numérique de Nantes, 44321 Nantes, France and Centre National de la Recherche Scientifique (CNRS), Nantes, 44321, France

Figure 1: The CRAFT prototype at the digital science lab, Nantes, France

vantages over rigid-link robots that fit very specific needs that were not yet addressed. They have been developed in many projects aiming to prove the feasibility of such systems in production environments and demonstrate their possible performance [12, 13]. However, the interest of such companies has so far mostly been limited to academic and R&D research, and several challenges, especially safety-wise, need to be overcome before CDPR actually enter workplaces.

While operating inside the robot's workspace, operators can often be surrounded by cables, and collision hazards not only occur because of the rigid moving platform, but also because of the cables. To ensure safety, collisions between the cables and the operator can be prevented, but this requires a precise knowledge of the system and the environment at all times. As the cables, due to the nature of such robots, span a large portion of the robot's workspace [14], this would restrict the possible movements and positions of both the operators and the robot. Hence, it is interesting to explore the possibility of tolerating collisions between the cables and the environment, including the operators, if the forces are light enough.

While very few works in the literature tackle the issue of cable-environment collisions, researchers have investigated internal collisions issues. Some analysis methods focused on modeling internal collisions to assess their impact on the robot workspace [15] and determine interference regions [16, 17]. Most of the work conducted so far focuses on avoidance based on path-planning. A continuous collision checking method was proposed for a CDPR boarding a robotic arm in [18]. This method, more effective than discrete methods, includes the detection of cable-cable collisions, cable-robot arm collisions, cable-platform collisions as well as robot-robot collisions. It can operate as an avoidance method when run before the motion, to validate a planned path, thus filling safety requirements, especially in preventing the robot from self-damaging. To avoid collisions between the robot and a cluttered environment, the concept of reconfigurable CDPR (RCDPR) using moving pulleys in order to modifiy the exit points of the robot was also proposed [19, 20]. Another method using Rapidly exploring Random Trees (RRT) considering both internal and external collisions was proposed in [21]. This was expanded with an AFT-RRT* algorithm simulated in a cluttered environment to obtain near optimal point-to-point motion in [22]. In the context of collaborative robotics, a method introducing a repulsive force in the admittance control, preventing two cables to fold onto one another [23].

Regarding external events and collisions, no interoceptive methods have been proposed so far, and the works proposing the detection of collisions with the environment or their avoidance usually rely on vision sensors or on model knowledge (pre-computed 3D model, SLAM, etc.) of the environment to adapt the path-planning to the obstacles currently in the workspace. However, these methods have drawbacks : they are subject to occlusion problems, are calculation-heavy, and/or require a exact knowledge of the environment. This limits the real-time capability of such systems, and prevent many collaborative uses where the operators may move or transport obstacles inside the workspace.

While internal collisions, between the cable themselves or between the cables and other moving parts of the robot, have already been studied, collisions between the cables and the environment were less documented and, to the knowledge of the authors, no detection method based on cable tension has been published yet. The main contributions of this paper lie in the introduction of a simple cable collision detection on cable-driven parallel robot and in the proposed safe control strategies, which can be chosen in order to mitigate such collisions.

This paper is organized as follows. Section 2 describes a model used to express the variation in cable tension resulting from cable collisions. This model is validated experimentally. After a presentation of the model of the CDPR used and its control in Section 3, Section 4 proposes a collision detection method relying on tension sensors and a tension distribution model. This method is validated experimentally in Section 5. Section 6 introduces a method to safely release a dangerously over-taut cable by redistributing the cable tensions and delimits its validity domain, with simulation results. Finally, conclusions about the work presented here are discussed in Section 7.

2. From collision forces to cable tension variations

In order to tolerate collisions, it is necessary to determine or at least to estimate the collision forces. Cables are, due to their flexible nature, difficult to instrument. A good understanding of the state of the cables can be obtained thanks to tension sensors placed at the end of the cables, at the anchor points of the moving platform. Modeling the behaviour of the tension in the cables during a collision is thus useful in order to monitor the robot at each timestep and assess each potential collision.

2.1. Limit collision forces

Harm hazards caused by collisions depend on the affected body part. A table expanding the various permissible pressures for each body part in the event of a quasi-static contact is presented in the appendices of the ISO/TS15066 standard. These biomechanical values were obtained in a study conducted by the University of Mainz on the pain onset levels [24]. The body

parts that are the most at risk in the use of the robot depend on the task and the robot configuration.

As the CRAFT prototype is a suspended CDPR, the upper body is most at risk, while cable collision risks with the lower body are very low.

Cables used in the prototypes of CDPRs made for collaborative use have a relatively small diameter. On the CRAFT platform, the cables used are VECTRAN VECT070LE, synthetic cables with a 0.7 *mm* diameter. Using a uniform pressure model, the collision force can be obtained by multiplying the pressure p_s by the contact surface. For a first approximation, this surface can be assumed to be a rectangle of a height corresponding to the diameter of the cable and a variable length (depending on the concerned body part). Depending on the body part, the maximum pressure and the typical contact area varies.

The head and the neck are particularly at risk, and would probably require some specific safety measures. Hence, these contacts are for now considered avoided and, for this study, the back of the hand is chosen, with a maximum pressure p_s.

$$p_s = 190 \text{ N/cm}^2 \tag{1}$$

Hands, while not being the most fragile body parts, generally offer a smaller contact area resulting in a smaller force necessary to obtain a equivalent pressure. They are also more often in contact with the cables since the operator may want to use them to move ease his or her way into the workspace. This more important risk exposure also argues in favour of the choice of this body part. A sketch of the contact is shown Fig. 2. Here the chosen contact area s_{co} is located at the side of the hand, with a contact length of $l_{co} = 15mm$, can be estimated as:

$$s_{co} = \varnothing_{ca}\, l_{co} = 10.5 \text{ mm}^2 \tag{2}$$

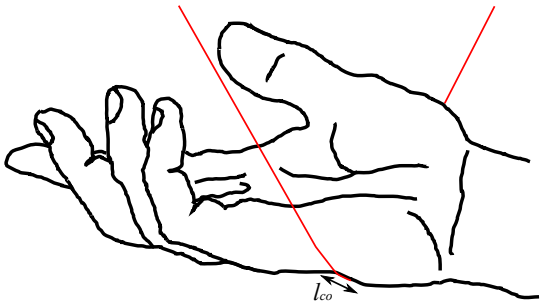

Figure 2: Contact length between a hand and a cable

This gives the maximum admissible contact force f_C^{adm} between the cables and a human operator. When this threshold is reached, there is a risk for the operator's safety and the robot needs to react accordingly so as to avoid or limit the damage.

$$f_C^{adm} = p_s\, s_{co} \approx 20 \text{ N} \tag{3}$$

2.2. Theoretical Model

When the operator or the environment collides with the cable, the latter is deformed by the external force applied on it. The collision will be detected via a measurement of the cable tension, when a dangerous change of the tension is observed. The purpose of the collision model is to establish a link between the force supported by human and the variation in cable tension. The model will allow to assess if this sensor is able to detect the collision or if the change of tension is too low and will thus be hidden by the noise in the measurement.

A cable-hand collision model is illustrated in Fig. 3. Here, the cable is assumed constrained between the points A and B, in a quasi-static configuration. The point A is the exit point of the cable, fixed to the main frame. On the CRAFT prototype, the angular position of the motors is servoed by the system. The point B is the anchor point, located on the moving platform. This platform can be assumed to be fixed due to the constraints of the other cables. However, in practice, a suspended cable robot has a compliance and the platform moves when the efforts applied on the cables are too important. However, this is a simple model which remains close to reality since such moves are limited.

In this figure, forces are drawn in red and lengths in black. The initial tension in the cable is noted τ. The lateral force $\mathbf{f_C}$ creates a deformation in the cable, resulting in a increased tension $\tau + \delta\tau$. Additional variables are needed, namely the cable length noted l, the Young modulus E and the cable section area S.

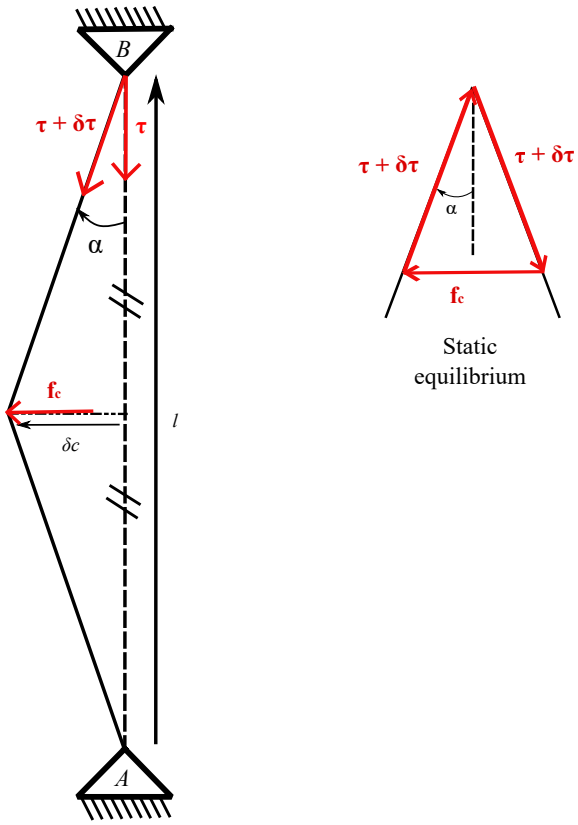

Figure 3: Model of a cable collision. Left : Geometric model. Right : Force equilibrium, static case.

Several other phenomena are neglected here, such as the own weight of the cables, or the creeping of the cables. The weight of the cables is negligible in front of the tension forces

in the cables. The creeping is neglected here because the collisions risk causing harm in less than a second, while the phenomenon in question takes more time to affect the system. However, in a prolonged crushing case, assessing its impact would be necessary.

Normalized values for the forces and the displacements are introduced here in order to simplify the equations. The normalized force f_{CR}, normalized cable tension τ_R and $\delta\tau_R$ for the cable tension variation are defined as follows :

$$f_{CR} = \frac{f_C}{ES}, \tau_R = \frac{\tau}{ES} \text{ and } \delta\tau_R = \frac{\delta\tau}{ES}$$

Additionally, the normalized lengths δ_{CR} for the relative lateral displacement and δl_R for the cable elongation can be defined:

$$\delta_{CR} = \frac{\delta c}{l} \text{ and } \delta l_R = \frac{\delta l}{l}$$

Normalized forces allow to remove the dependency in the cable characteristics ES and with normalized lengths, the dependency of the following calculus in the cable characteristics and the cable length is also removed, allowing a generalization to all cable types and platform poses.

Cable elasticity model. The model presented in Fig. 5 defines the relationship between the collision force, the initial cable tension and the resulting variation in cable tension.

The increase in tension in the cable can simply be obtained using Hooke's law. The relative elongation of the cable resulting of the collision, noted δl_R is directly proportional to the force increase value $\delta\tau$. With the normalized tension increase, this simplifies as :

$$\delta\tau_R = \delta l_R \tag{4}$$

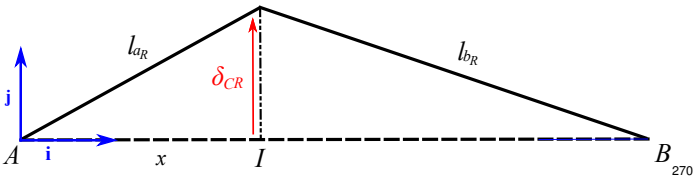

Figure 4: Geometric model of the elongation δl

Cable elongation. The cable elongation can be defined as a function of the lateral displacement δ_{CR} through a simple geometric model of the cables. This geometric model is shown in Fig. 4.

The elongation δl_R can be written, defining x such that $|AI| = x$. The parameter x varies from 0 to 1 depending on the position of the contact point I on the cable segment $[AI]$.

$$l_{aR} = \frac{l_a}{l} \text{ and } l_{bR} = \frac{l_b}{l} \tag{5}$$

$$\begin{aligned} \delta l_R &= l_{aR} + l_{bR} - 1 \\ &= \sqrt{\delta_{CR}^2 + x^2} + \sqrt{\delta_{CR}^2 + (1-x)^2} - 1, x \in [0,1] \end{aligned} \tag{6}$$

By derivation of this function $\delta l_R(x)$, it can be noticed that the elongation is minimal when $x = \frac{1}{2}$. This minimum results in a minimal cable tension increase, hence, this corresponds to the worst case scenario regarding the detectability of cable collisions. Indeed, a same collision force would lead to a more significant tension increase applied at the ends of the cable, easier to detect by monitoring these cable tensions, than if applied at the middle. Moreover, the shape of the $\delta l_R(x)$ function is shown Fig. 6 for force and tension values corresponding to typical uses of the prototype. This figure shows that the elongation does not vary significantly near the middle point.
With $x = \frac{1}{2}$, the elongation function can be simplified :

$$\delta l_R = -1 + 2\sqrt{\delta_{CR}^2 + \frac{1}{4}} \tag{7}$$

Cable lateral displacement. The relationship between the norm of the lateral force f_{CR}, the initial cable tension τ_R, and the relative lateral displacement δ_{CR}, valid when the latter is small enough, is expressed as follows :

$$f_{CR} = 8\,{\delta_{CR}}^3 + 4\,\tau_R\,\delta_{CR} \tag{8}$$

This equation is obtained through the geometric model of the cable presented above and the static equation balancing the internal normalized force depending on the elongation of the cable and the normalized external force applied at the middle point of the cable [25]. The middle point is chosen because, as shown above, it corresponds to the least sensitive collision detection. The details of the derivation of the formula are given in Appendix A.

From this equation, given a f_C value, for instance f_C^{adm}, corresponding to a normalized force ${f_{CR}}^{adm}$, a relative displacement δ_{CR} can be found by solving the third order polynomial equation. This is a depressed form, where Cardano's formula can be used. Equation (8) can be rewritten, to match the canonical form for the equation :

$${\delta_{CR}}^3 + \frac{1}{2}\,\tau_R\,\delta_{CR} - \frac{1}{8}\,f_{CR} = 0 \tag{9}$$

Then the discriminant of the depressed cubic form Eq. (9) can be computed, giving the nature of the roots of the polynomial. Since the normalized forces τ_R and f_{CR} are always positive, this cubic has two complex conjugate roots and a unique real root which is the physical solution of the problem. The latter can then be calculated:

$$\delta_{CR} = \sqrt[3]{\frac{f_{CR}}{16} + \sqrt{\frac{{f_{CR}}^2}{256} + \frac{{\tau_R}^3}{216}}} + \sqrt[3]{\frac{f_{CR}}{16} - \sqrt{\frac{{f_{CR}}^2}{256} + \frac{{\tau_R}^3}{216}}} \tag{10}$$

Then, by combining Eq. (4, 7, 10), the following equation is obtained, linking the collision force and the initial cable tension with the variation of cable tension :

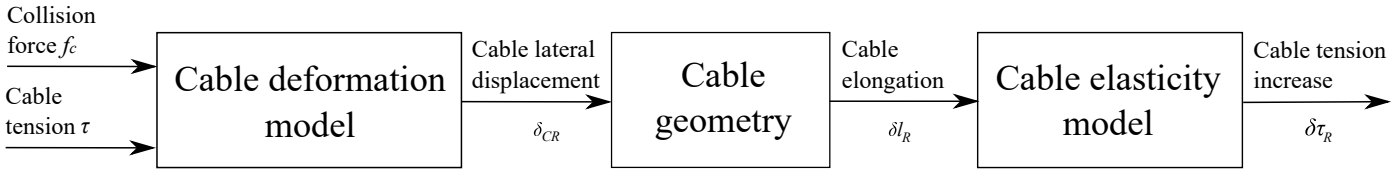

Figure 5: From the collision forces to the cable tension increase : theoretical model

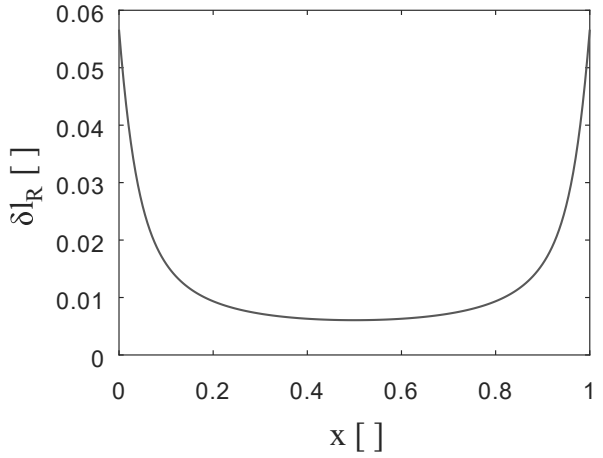

Figure 6: Elongation curve, in function of the longitudinal position factor x of the application point of the lateral force, for $\tau = 30$ N, $f_C = 20$ N and $ES = 1,8 \times 10^4$ N, typical values for the CRAFT prototype.

$$\delta\tau_R = \Bigg[-1 + 2\Bigg(\left(\frac{f_{CR}}{16} + \sqrt{\frac{{f_{CR}}^2}{256} + \frac{{\tau_R}^3}{216}}\right)^{2/3} + \left(\frac{f_{CR}}{16} - \sqrt{\frac{{f_{CR}}^2}{256} + \frac{{\tau_R}^3}{216}}\right)^{2/3} - \frac{1}{4}\Bigg)^{1/2}\Bigg] \quad (11)$$

Hence, by knowing the collision force and the initial cable tension, the cable tension increase resulting of the collision can be predicted. An admissible increase of tension corresponding to a pressure applied by the cable on the human inferior to the acceptable pressure defined in the standard (found in [24]) can be thus defined.

2.3. Validation of the model

In order to validate the strategy proposed in the previous part, the model proposed in [25] must be verified experimentally. To do so, a test bench is proposed, followed by an experiment and an analysis of the results.

To validate the model of lateral deformations in the cable, a test bench respecting the hypotheses of the problem can be designed. This device must allow the measurement with a reasonable precision of the lateral displacement δc, the total length of the cable l, the cable tension τ in the cable and the lateral force f_C. A test bench is designed using a workbench on which two clamping vices and a winch are fixed, to reproduce the constraints on the cables on the prototype and to generate lateral efforts, with the adapted sensors. A sketch of the test bench is shown Fig. 7.

The *Clamping vice 1* represents the anchor point of the cable on the platform. On this clamping vice is fixed the *Dynamometer 1*, that will allow measuring the tension τ and $\tau + \delta\tau$ in the cable tied to it in all configurations, figuring the boarded tension sensor. The *Clamping vice 2* boards a second dynamometer used to measure the generated lateral forces $\mathbf{f_C}$. These forces are generated by simply moving the mobile jaw of the clamping vice of a measured displacement. Both devices are RS PRO 196N numerical dynamometers, whose range cover the feasible tensions of the CDPR prototype used at the LS2N. The *Winch* represents the exit point of the cable. Its longitudinal position on the bench, measured with a ruler, defines the length l. Once in position, turning the winch sets the tension in the cable as would the motor - drum - pulley assembly do on the robot.

All the forces are measured in the plane Π, parallel to the plane of the workbench, defined by the vectors $\mathbf{i}$ and $\mathbf{j}$. This implies that all the points where the cables are connected are located in this plane Π.

The results of the experiment including the measured current tension values $\tau + \delta\tau$ in the cable, after a lateral force f_C is applied, are shown Fig. 8, for the Vectran VECT070LE cable. These measured tension values can be compared in these plots to the ones drawn from the mapping shown Eq. 11.

Since the exact values of the cable characteristics ES are not precisely known, the theoretical curves are fitted to the data by adjusting the value of the ES product. The red dots are the experimental measures and the colored map are the values calculated thanks to the theoretical model. This experiment shows that the experimental values follow closely the theoretical model, while some errors exist outside of the calculated uncertainties, hinting that some error sources are ill-known. The ES value obtained by fitting the curve is 1.0×10^4 N. This value can then be compared to the theoretical value given by the supplier : 2.9×10^4 N. While this value is in the same order of magnitude, there is a factor 3 difference between the experimental and the theoretical. However the values of ES are difficult to be identify and often depend on the experimental conditions (previous load, repeated bending, current tension). Hence, Zhu and Meguid recommend in [26] to measure the elastic modulus of the cable in conditions similar to the ones of the working process. This implies that the ES value needs to be computed again on the robot itself for better results.

Slices of the 3D maps obtained above for particular lateral

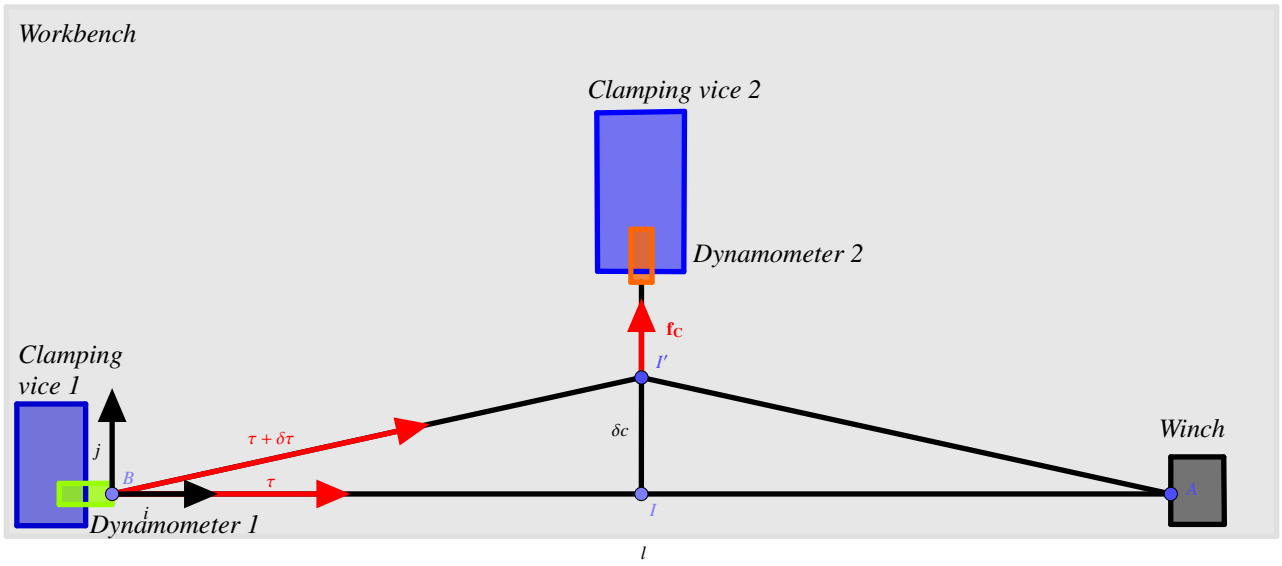

Figure 7: Sketch of the test bench

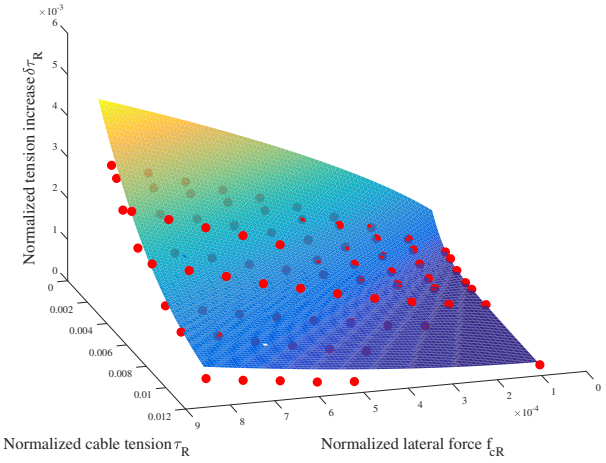

Figure 8: Theoretical and experimental values of $\delta\tau$, for $\tau \in [1, 140]$ N and for $f_C \in [0, 10]$ N for a Vectran VECT070LE $\varnothing_{cable} = 0.7$ mm cable.

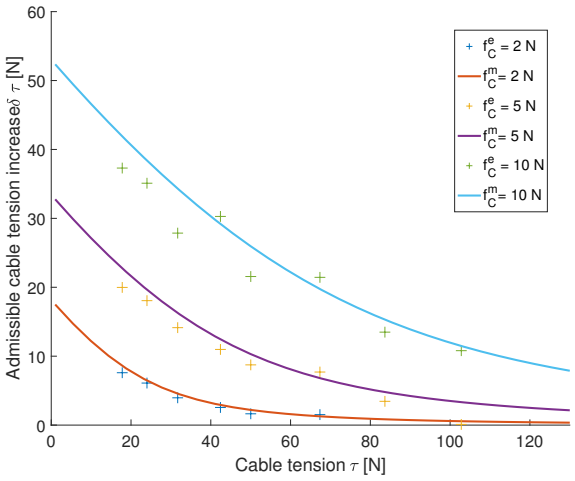

Figure 9: Experimental and theoretical curves of $\delta\tau$ for the Vectran VECT070LE cable in terms of f_c values. Continuous lines for fixed f_c^m values correspond to the curves obtained with the model and plots with fixed f_c^e values are the points corresponding to the experimental results.

force values are plotted in Fig. 9 for readability. Here, each curve or set of experimental point corresponds to a fixed value of f_c, noted f_c^m for the model curves and f_c^e for the experimental points.

The error is defined as the absolute difference between the theoretical and the experimental points $e_{\delta\tau} = \frac{|\delta\tau_{th} - \delta\tau_m|}{\delta\tau_{th}}$. The highest errors are obtained for low cable tensions with a quasi-linear dependence in the lateral force. After removing the outliers, the average error is $e_{\delta\tau} = 14\%$, and the highest error is $e_{\delta\tau,max} = 42\%$. While these are important proportions errors, these only correspond to a couple Newtons in absolute errors. Moreover, the highest error corresponds to a case with a high cable tension (100 N) and a low collision force (2 N), far from the use case of this study. This however shows the limits of the approach for such cases.

In these figures, the difference which can be noticed between the theoretical and experimental values remains below 5 N, and the shape of the calculated map seems close to the one formed by the experimental points. A part of this difference may be due to cable creeping, i.e. the loss of tension over time in a taut cable, which is no longer negligible for the time scale of a measurement series.

Two other cables, a Dyneema DYNE083LE (textile) and a

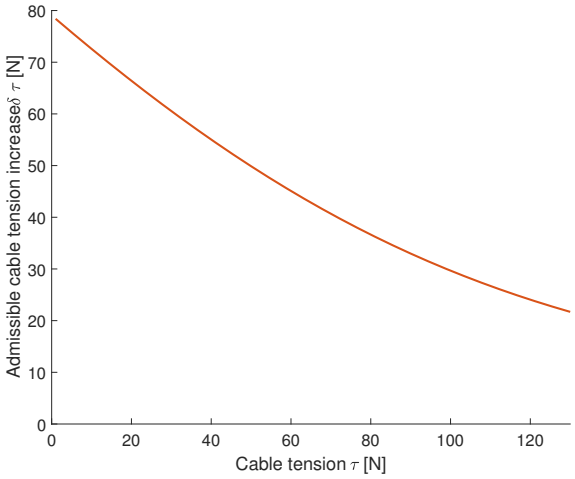

Figure 10: $\delta\tau$ threshold value depending on the cable tension τ for $f_C^{adm} = 20\,\text{N}$ with a Vectran VECT070LE cable, $ES = 1 \times 10^4\text{N}$

CarlStahl CG07_2045 (steel), were tested but the results are not reproduced here due to a lack of space, with lower maximal errors for the steel cable. This can be explained by the relatively low influence of the creeping effect on steel cables compared to the textile ones [27].

2.4. Conclusion

In conclusion, the experiment has confirmed the proposed theoretical model, which gives a satisfying estimate of the evolution of the tension in the cable when a lateral force is applied on it once the cable characteristic parameters are correctly identified. The experiment also identified working values for the ES product.

Using the model estimate, it is then possible to create a first implementation of a collision detection system with a tolerance. While the robot is operating, the real increase in tension value $\delta\tau_{measured}$ obtained through sensors can be compared to the value extracted from the curve displayed in Fig. 10 in order to determine whether this collision exceeds the admissible force value or not (here 20 N). This curve extrapolates the fitted curve for the VECT070LE cable and will thus be used as a reference for the implementation on the prototype. It must be noted that this tension variation does not depend on the cable length. However, in order to build a working system despite the errors, some experiments on the prototype will be necessary in order to adjust the curve depending on the real system stiffness.

3. CDPR Modeling and control

In order to implement the collision detection, the cable robot needs to be modeled so that an appropriate control scheme can be defined. The precision of this model must allow to discriminate between cable tension variations due to the movement of the robot and external variations due to collisions. Elements regarding the geometric and static modeling of the robot are presented here.

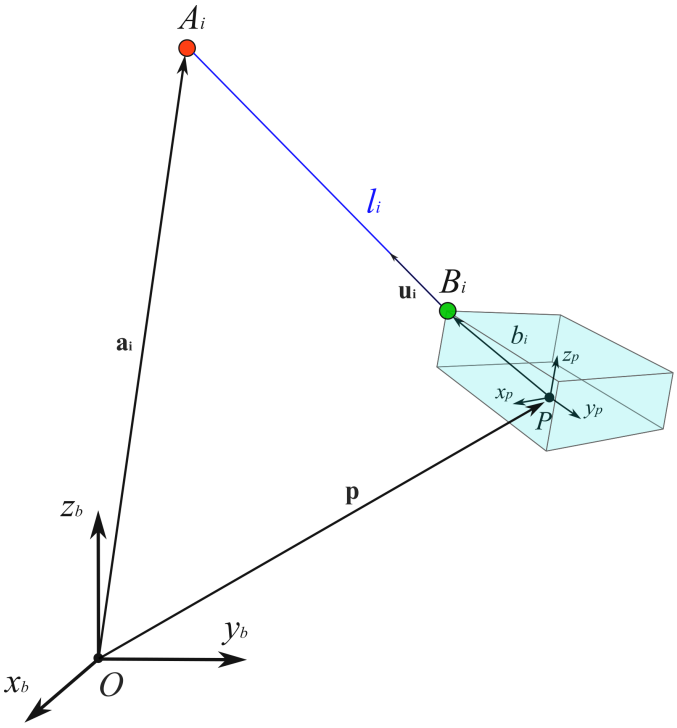

Figure 11: Architecture of a CDPR

3.1. Geometric and dynamic model of the CDPR

A CDPR consists of a platform, a main frame and a set of m cables. These connect the anchor points B_i, $i \in \{1, m\}$ of the platform to the end points A_i corresponding to the pulleys on the main frame. The length l_i of the cables is determined by the angular position q_i of the motors controlling the drums.

O is the origin of the main reference frame $\mathcal{F}_b$, and P is the origin of the moving platform's reference frame $\mathcal{F}_p$. The vectors $\mathbf{a}_i$, indicating the position of the end point A_i in $\mathcal{F}_b$, $\mathbf{b}_i$, indicating the position of the anchor point in $\mathcal{F}_p$ and $\mathbf{p}$, pointing the current position of the platform in $\mathcal{F}_b$, are used in the geometric loop closure. The unit vector $\mathbf{u}_i$ points the direction of the cable between A_i and B_i. These geometric parameters are shown Fig. 11. For readability purposes, only cable i is displayed, even though the prototype studied here has $m = 8$ cables.

The following static equation ensures the static equilibrium of the mobile platform :

$$\mathbf{W}\tau + \mathbf{w}_{ext} = 0_6 \tag{12}$$

Where $\mathbf{W}$ is Wrench matrix, where $\boldsymbol{\tau}$ is the cable tension vector and where $\boldsymbol{w}_{ext}$ is the wrench of the external forces, including the gravity.

The Wrench matrix of the robot is defined as following [10]:

$$\mathbf{W} = \begin{bmatrix} \mathbf{u}_1 & \dots & \mathbf{u}_i & \dots & \mathbf{u}_m \\ \mathbf{b}_1 \times \mathbf{u}_1 & \dots & \mathbf{b}_i \times \mathbf{u}_i & \dots & \mathbf{b}_m \times \mathbf{u}_m \end{bmatrix} \tag{13}$$

It is possible to isolate the platform in order to determine its dynamic equation. To do so, the inertia matrix of the platform

$\mathbf{I}_p$, the Coriolis matrix $\mathbf{C}$, its operational acceleration vector[3] of the platform $\ddot{\mathbf{x}}$ and the velocity vector of the platform $\dot{\mathbf{x}}$ need to be introduced in order to obtain the following result :

$$\mathbf{I}_p(\mathbf{x})\ddot{\mathbf{x}} + \mathbf{C}(\mathbf{x}, \dot{\mathbf{x}}) = \mathbf{W}\boldsymbol{\tau} + \mathbf{w}_{ext} \tag{14}$$

3.2. Actuation of the CDPR

Cable lengths are required to calculate the Wrench matrix $\boldsymbol{W}$. These can be obtained knowing the angular position q, assuming that the cable is non-elastic. The latter follows the dynamic equilibrium related to the motorization of the robot, established at the output of the gearbox, shown Eq. (15). A Coulomb viscous friction model was chosen to estimate the friction of the shaft, regrouping the friction inside the motor, the gearbox and the pivot links. The friction coefficients in the actuators were determined experimentally. In the following equation, $\mathbf{I}_m$ is the inertia matrix of the motor and gearbox calculated at the gearbox output, $\mathbf{f}_s$ is the static friction coefficient vector, $\mathbf{f}_v$ the fluid friction coefficient vector, both of size $m = 8$[4], r_d the radius of the winches and τ is the vector of cable tensions $\tau_i,\ i \in [1, m]$. $\boldsymbol{\Gamma}_{mg}$ is the vector of torques generated by the motor and gearbox assembly $\Gamma_i,\ i \in [1, m]$. The Hadamard product multiplying vectors $\mathbf{u}$ and $\mathbf{v}$ element-wise is noted $\mathbf{u} \odot \mathbf{v}$.

$$\mathbf{I}_m\ddot{\mathbf{q}} + \mathbf{f}_s \odot sign(\dot{\mathbf{q}}) + \mathbf{f}_v \odot \dot{\mathbf{q}} + r_d\ \boldsymbol{\tau} = \boldsymbol{\Gamma}_{mg} \tag{15}$$

Using the dynamic model Eq. (14,15), a computed torque control law is built to servo the angular position of the winches $\mathbf{q}$. The desired position is noted $\mathbf{q}^d$ and the angular error is defined $\mathbf{e}_q = \mathbf{q}^d - \mathbf{q}$. The closed-loop behavior of the error should follow, with K_p, K_v, K_i the gains of the system :

$$\ddot{\mathbf{e}} + K_v\ \dot{\mathbf{e}} + K_p\ \mathbf{e} + K_i \int \mathbf{e} = 0 \tag{16}$$

$$\ddot{q}_i = \ddot{q}_i^d + K_v\ \dot{e}_i + K_p\ e_i + K_i \int e_i \tag{17}$$

Hence, for each cable i, the angular acceleration can be computed, allowing the computation of torque $\boldsymbol{\Gamma}_{mg}$ using Eq. (15), provided the desired cable tension $\boldsymbol{\tau}$ is known.

3.3. Tension distribution

The studied CDPR is a redundantly-actuated system with $m = 8$ cables and $n = 6$ degrees of freedom, resulting in an actuation redundancy of $r = m - n = 2$, corresponding to the dimension of the solution set[28]. Hence, there is an infinity of solutions for the cable tensions generating the movements of the platform and a force distribution method is necessary to find an feasible solution balancing the system and avoiding cable slackness.

Cable tensions must be constrained within an interval between the minimum and the maximum admissible tensions. A Tension Distribution Algorithm (TDA) allows to enforce these constraints. There are several approaches to calculate the force distributions, using optimization, linear or quadratic programming or barycenter methods. A list of different approaches and their comparison is presented in [29]. All solutions can be written, from Eq. (14), by neglecting the Coriolis and acceleration term since the robot is operating at low speeds and accelerations:

$$\boldsymbol{\tau} = -\mathbf{W}^+\mathbf{w}_{ext} + \mathbf{N}\ \boldsymbol{\lambda} \tag{18}$$

Where $\mathbf{W}^+$ is the Moore-Penrose pseudo-inverse of the matrix $\mathbf{W}$ of size (6×8) and of rank 6 for a robot with $m = 8$ cables[5], $\mathbf{N}$ is the kernel of the wrench matrix $\mathbf{W}$, of size (8×2), such that $\mathbf{W}\mathbf{N}\boldsymbol{\lambda} = \mathbf{0}_6$.

The choice made here is to minimize the energy consumption by minimizing the norm of the cable tension vector. Moreover, in the scope of ensuring the safety of operators comanipulating with the robot, minimizing the cable tensions reduces the risk of dangerous collisions and eases their detectability since the lower the cable tension, the higher the admissible tension increase in case of collision, as shown above. Hence, vector $\boldsymbol{\lambda}$ is of dimension 2 and determined such that :

$$\begin{aligned} \underset{\boldsymbol{\lambda}}{\text{minimize}} \quad & \|\boldsymbol{\tau}(\boldsymbol{\lambda})\|^2 \\ \text{subject to} \quad & \tau_i \geq \tau_{min}, i \in [1, .., m] \\ & \tau_i \leq \tau_{max}, i \in [1, .., m]. \end{aligned} \tag{19}$$

For the prototype at hand, $\tau_{min} = 0$ and $\tau_{max} = 80$ N. This value was chosen according to the maximum output torque provided by the motors. In most of the robot workspace, the solution is $\boldsymbol{\lambda} = \mathbf{0}_2$ for the suspended robot studied here. The case $\boldsymbol{\lambda} = \mathbf{0}_2$ corresponds to the solution given only by the pseudoinverse of the wrench matrix.

In Fig. 12, the static equilibrium poses which can be reached satisfying the constraint $0 \leq \tau_i \leq \tau_{max}, i \in [1, .., m]$ regardless of the value of $\boldsymbol{\lambda}$ are plotted in purple while the poses where $0 \leq \tau_i \leq \tau_{max}, i \in [1, .., m]$ and $\boldsymbol{\lambda} = 0$ are plotted in green.

3.4. Control law

The complete control law can thus be computed. Angular accelerations of the motor shafts, conversely to the Cartesian accelerations of the platform, cannot be neglected.

$$\begin{aligned} \boldsymbol{\Gamma}_{mg} = \mathbf{I}_m \Big(& \ddot{\mathbf{q}}^d + K_d\ \dot{\mathbf{e}} + K_p\ \mathbf{e} + K_i \int \mathbf{e} \Big) \\ & + \mathbf{f}_s \odot sign(\dot{\mathbf{q}}) + \mathbf{f}_v \odot \dot{\mathbf{q}} \\ & + r_d\ (-\mathbf{W}^+\mathbf{w}_{ext} + \mathbf{N}\ \boldsymbol{\lambda}) \end{aligned} \tag{20}$$

A view of the control scheme is presented Fig. 13. The motors of the CDPR are controlled by torques, but the desired input and the return are angular positions corresponding to cable lengths. With such a control law, the expected tension inside the cables is given by :

$$\boldsymbol{\tau}_{ff} = -\mathbf{W}^+\mathbf{w}_{ext} + \mathbf{N}\ \boldsymbol{\lambda} \tag{21}$$

[3] The operational acceleration vector of the moving-platform is a six-dimensional vector containing its linear and angular acceleration vectors.

[4] Coefficients differ from one motor shaft to another

[5] Assuming that the robot is not in a singular configuration.

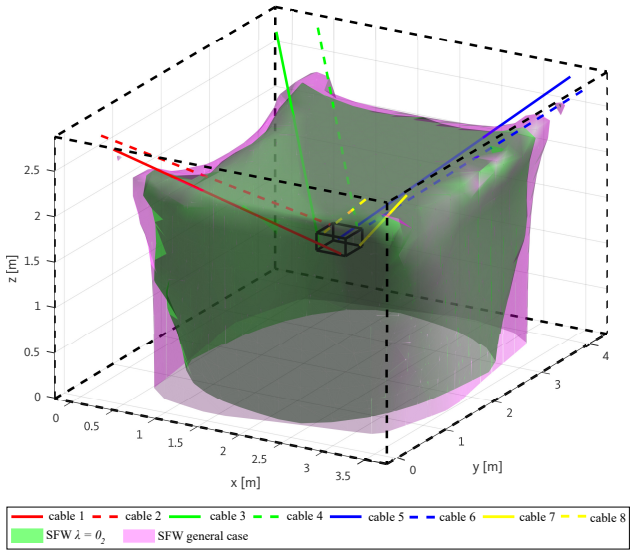

(a) 3D view of the SFW

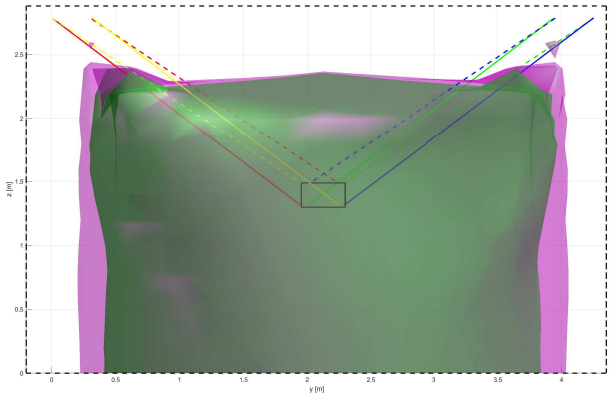

(b) Side view of the SFW

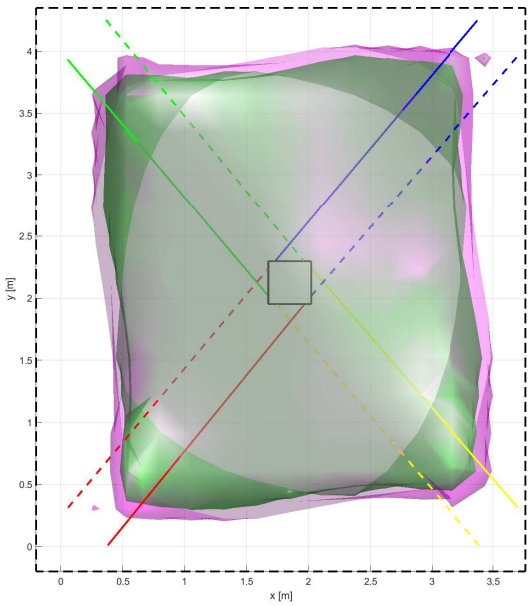

(c) Top view of the SFW

Figure 12: In purple : Static Feasible Workspace of the robot. In green : approximation of this workspace using the pseudoinverse of the wrench matrix $\mathbf{W}$ (case $\boldsymbol{\lambda} = 0_2$). Only solutions returning positive and bounded cable tensions are kept. The approximation $\boldsymbol{\lambda} = 0_2$ is included in the real SFW. The latter uses different λ values, allowing higher cable tensions able to satisfy Eq. (19).

4. Cable collision detection

In order to perform the collision detection, the model must first be validated. A first experiment is conducted on the prototype, monitoring a trajectory and the difference between predicted and measured values of the cable tensions. The implementation on the prototype is briefly described below.

4.1. Implementation

The tension sensors. The cable tensions are measured using 8 FUTEK FSH04097 sensors, one for each cable, tied to the cables at the anchor points of the platform, as shown in Fig. 14. Their signal is amplified using 8 FSH03863 voltage amplifiers and sent the robot controller by a coaxial cable. Their measurement frequency is 1 kHz, but these sensors are able to provide with tension values at a frequency up to 5.3 kHz.

The platform. The sensors are boarded on the robot mobile platform which consists of an 8-anchor points parallelepiped made of aluminum profiles. This platform also boards the amplifiers and a board centralizing the information of the sensors for transmission to the robot control.

dSpace controller. The dSpace controller consists of several modules connected to a PX10 expansion box, which centralizes the information of all the encoders and the other sensors. This box communicates with a control PC connected via Ethernet connection.

ControlDesk. The control PC runs an instance of dSpace ControlDesk, a highly configurable interface that provides the system with a Human-Machine Interface, displaying information about the current state of the robot and allowing its control.

Numerical filtering. Some of the data collected by the sensors requires filtering before being used in the control of the robot. This is the case for the tension signal provided by the tension sensors mentioned above, which is highly noised.

A numerical filtering is thus used, based on a digital Infinite Impulse Response filter. A 5-th order Butterworth set of coefficient is chosen to implement a sufficiently selective low-pass filter. The chosen cut-off frequency is $f_C = 10$ Hz for a normalized cutoff frequency of $\omega_n = 2\frac{f_C}{f_s}$, with the sample frequency $f_s = 1000$ Hz.

Corrector gains. The corrector gains K_p, K_d and K_i are determined using the Ziegler-Nichols tuning method. Values of the gains are summarized in Tab. 1.

Table 1: Corrector gains

Coefficient	Value
K_p	4.0529×10^4
K_v	348.69
K_i	1.5702×10^6

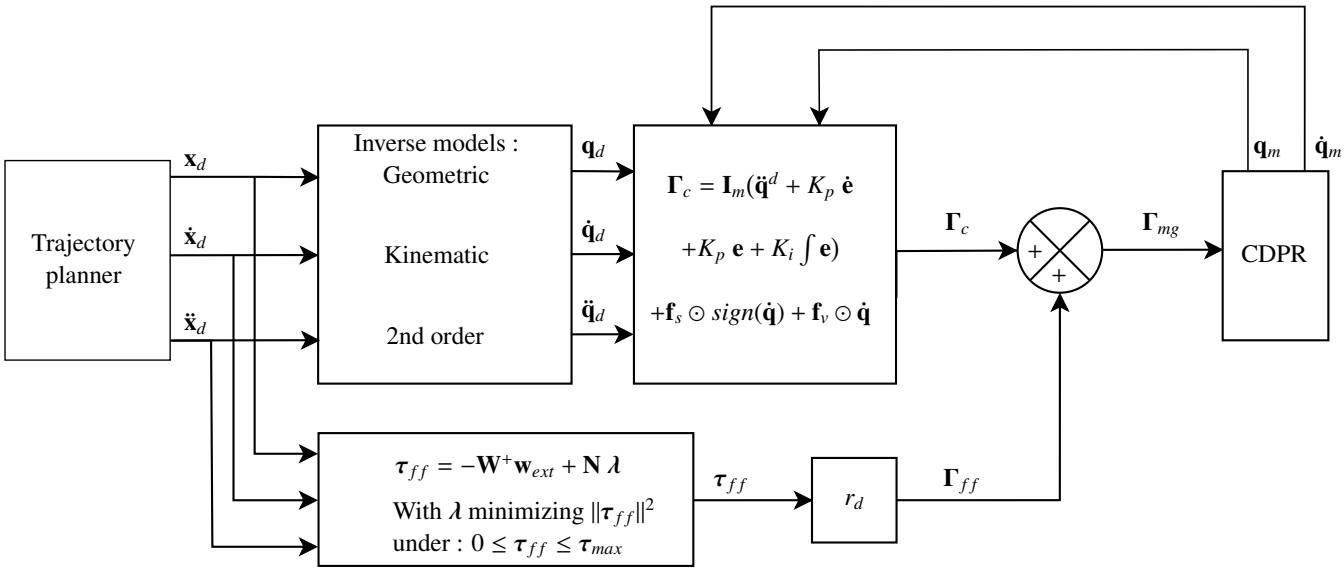

Figure 13: Control scheme of the CDPR with the pseudo-inverse tension distribution

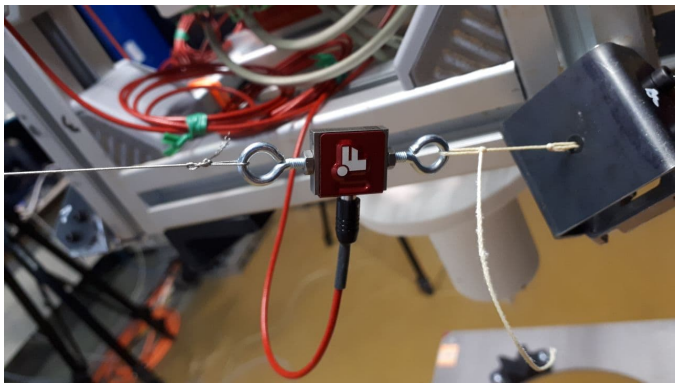

Figure 14: Tension sensor mounted on an anchor point of the platform.

4.2. *Validation of the control model*

The control scheme of the CRAFT prototype computes the expected cable tensions with the $\boldsymbol{\tau}_{ff}$ anticipation term. Both values are plotted during a circular trajectory around the center of the workspace Fig. 15. Only one cable is featured for readability, but while tension profiles tend to change depending on the cable, the difference between the predicted and the measured tensions is overall similar. For reference, the tension profiles in the other cables along the trajectory is plotted Fig. 16.

While the tension computed with the robot model and the tension measured by the sensors have the same shape and the values remain close, a difference is observed on this graph between the estimated values $\boldsymbol{\tau}_{ff}$ and the measured ones $\boldsymbol{\tau}_m$, because of model errors. These are first due to the imprecise knowledge of the friction model and the lack of an elasticity model of the cables which imply a reduced positioning accuracy resulting in model geometry errors, especially in the computation of the Wrench matrix. Adding such an elastic model has shown important accuracy improvements for suspended CDPRs [30].

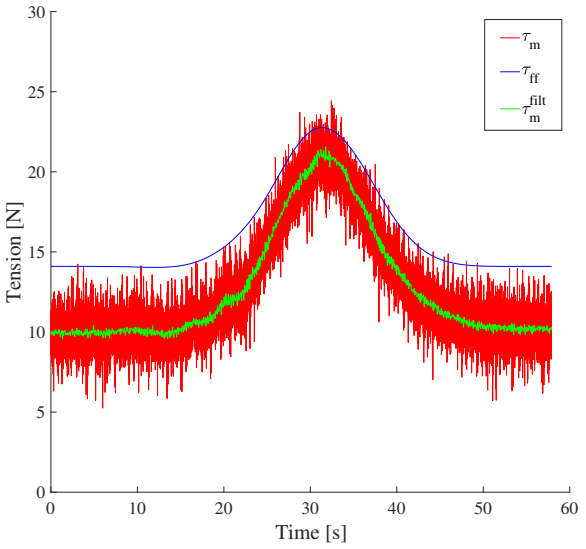

Figure 15: Comparison of the predicted and measured tensions on a circular trajectory - Cable n°1

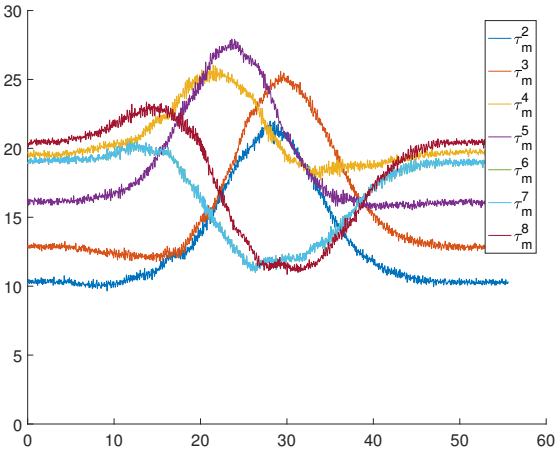

Figure 16: Tension profiles on Cables n°2 to 8 along the circular trajectory

Neglecting the acceleration and Coriolis terms also induces errors on the model, however, the error is more significant when the cable is stopped, suggesting a predominant impact of the friction model over the errors related to the dynamic effects. It must be noted that the Coulomb friction model used here does not allow predicting the friction forces when the actuator velocities are null, explaining the larger errors at both ends of the trajectory corresponding to the tension profile shown in Fig. 15. Regardless of the error sources, since this difference is about few Newtons, a collision detection system based on the model proposed above can operate in spite of those inaccuracies.

Thus, an adapted collision detection strategy can be designed based on the cable tension prediction and the measured values.

4.3. Collision detection strategy

A simple collision detection strategy would be to monitor the difference between the tension output from the dynamics feed-forward block, noted $\boldsymbol{\tau}_{ff}$, and the measured cable tension. When this one overshoots an error threshold, a collision can be declared. However, this collision may or may not be dangerous.

As proposed earlier, it is possible to ensure that the collision force remains under a certain safety threshold using the cable deformation model presented in Section 2. While this could theoretically be done using the values found there, in practice, the threshold curve is different than the one determined for the test bench, since the *ES* product depends on the setup. Hence, the system needs to be calibrated.

4.4. Calibration of the detection system

To do so, this collision model is first calibrated using a dynamometer. The calibration procedure consists in measuring a series of cable tensions with the tension sensors presented in this section, while applying a known lateral force $\mathbf{f}_c$ of a value corresponding to the collision threshold at the middle point of the cable. The measures are realized at different poses that imply different initial cable tensions.

The collision force model shows that the tension increase in the cable resulting of a lateral force does not depend on the cable length but on the contact force, the initial tension and the relative position of this contact. Assuming that the friction in the axis of the pulley sheave is negligible, cable tensions on both sides of the pulley are equal. Hence, the lateral force can be applied between the drum and the exit point and not directly between the exit point and the anchor point of the cable. It should be noted that the midpoint between the drum and the pulley can be marked and read easily. Thus, this choice allows to simplify the experimental setup and to increase the repeatability of the experiment. Moreover, applying the force on the side allows to keep a safe distance with the platform.

Hence, the measures are done by simply pulling the cable at the height marked on the plank fixed to the main frame shown Fig. 17. The cable is pulled slowly so as to remain in a quasi-static case.

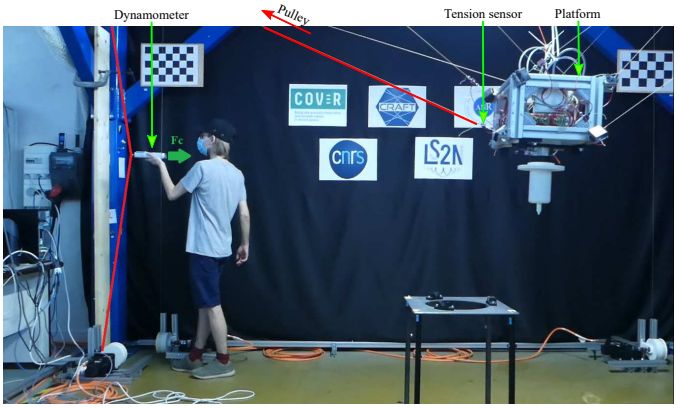

Figure 17: Calibration Procedure. In red : the cable on which is applied the lateral force $\mathbf{f}_c$ with the dynamometer. The dynamometer, tension sensor and platform are marked by a green arrow.

The measured values are then plotted using MATLAB and the model curve described above is fitted so as to correspond to these values. The resulting curve equation is then used in the robot parameters to define the collision threshold. The obtained calibration curve is presented Fig. 18.

The calibration procedure returns a curve allowing noticeable tension variations in case of collision between the cable and its environment. However, the equivalent stiffness parametrizing the curves is significantly lower than the value obtained in Section 2 found when the cable is taut and tied on both ends. On the prototype, the corresponding *ES* value is equal to 625 N only.

The loss of stiffness with respect to the previous experiments can be explained by the following points: small displacements of the platform when a cable is subject to an important lateral force were neglected in the model, the coupling effect between the cables and the regulation of the motor angular position.

However, the calibration provides with a knowledge of the relevant parameters for the collision detection on the prototype, regardless of the factors affecting the robot stiffness.

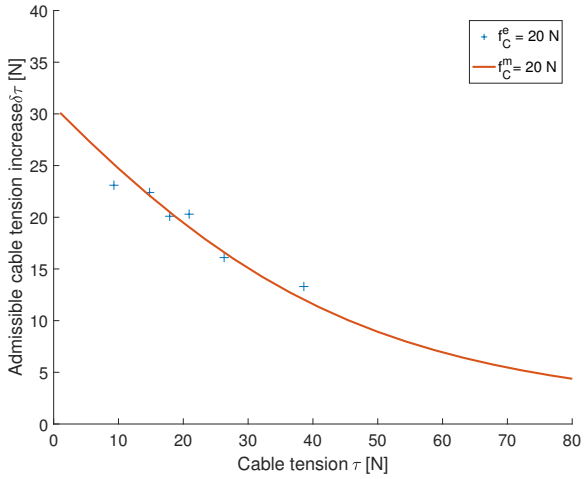

Figure 18: Calibration curve for the collision detection model, for a collision threshold of 20N.

5. Experimental validation of the collision detection

To assess the feasibility of the proposed collision detection method and to evaluate its performance, several experiments were conducted.

5.1. Experimental setup

This experiment was then made with the platform accomplishing a circular translation around the center of the workspace, in a horizontal plane 1.3 m above ground. Two different types of collisions were tested : brief impacts of various force values, and continuous collision with a progressively increasing force. The first ones are made to simulate brief collisions, while the seconds aim at reproducing crushing situations. [6]

In any case, when the collision is detected, the robot is stopped using an emergency stop, cutting all power and triggering the breaks. However, in a real implementation, the robot would likely not perform an emergency stop but rather a safety-monitored controlled stop or one of the other mitigation strategies described in Section 6.

A lateral force is then applied with a dynamometer at the middle of the cable on the section between the winch and the pulley. The setup is similar to the calibration procedure pictured Fig. 17.

The first recording was made for an control experiment, the platform performing the circular translation motion without any exterior perturbations. This allows to observe the contribution of the rise of tensions due to the robot motion only.

[6] While brief and repeated collisions could be considered outside of the quasi-static case, the stiffness of cables tend to increase when these are subject to dynamic excitation [31]. This increased stiffness will result in higher tension increases for equal collision forces and will hence be more detectable, the quasi-static case constituting a worst case with regard to this detectability criterion.

5.2. Results

A video of the 3 experimental setups was shot[7] and the evolution of the tensions plotted in the video is reproduced in Fig. 19 and Fig. 20. In order to asses the repeatability of the desired behavior, ten similar experiments were run, all leading to similar results.

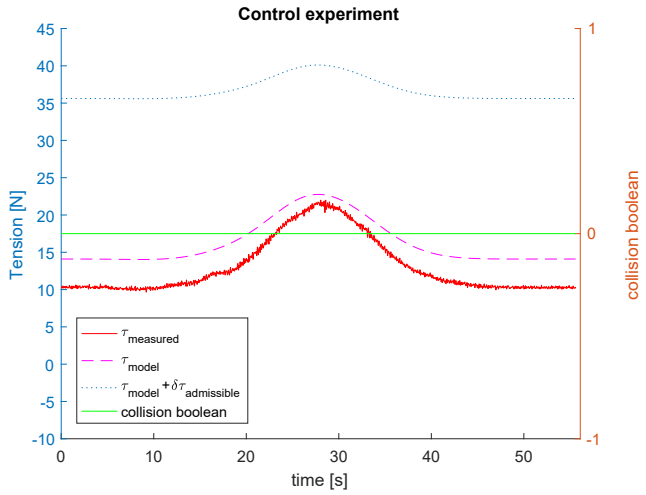

Figure 19: Evolution of the tensions in the cable 1 during a circular translation.

A first criteria to assess whether the proposed detection method is effective or not is to validate if, after calibration, it can successfully and reliably detect dangerous over-tensions.

The tension curves are displayed in Fig. 20 for the control, multiple collisions and crushing trajectories respectively. The collision detection system effectively detects the overshooting of the variable tension threshold, since the green signal representing the collision state boolean of the first cable effectively switches to one when the measure signal crosses the threshold. This results in the robot prototype cutting immediately the power and triggering the breaks, as it can be seen on the video of the experiment. This behavior was tested successfully multiple times.

The events determining the response time are the rising edge of the collision boolean and the crossing of the admissible tension threshold. However, the measured cable tension signal oscillates in a ±2 N range, implying a less precise reading. In order to minimize the impact of these reading errors, several measures are averaged. No significant difference is found for the reaction time between the collision and the crushing case. Overall, eleven collisions experiments were run to assess the repeatability of the detection and to determine more precisely the reaction time. The reaction times are summarized in Tab. 2. On average, the reaction time is 52 ms, with a standard deviation of 20 ms, corresponding to 52 times the sampling period. Hence, the system is able to react in a much shorter time than the duration separating the short collision case (transient event) and the crushing case (quasi-static event) in the ISO/TS 15066 standard [24], *i.e.* 500 ms.

[7] The experiment video can be watched here : `https://youtu.be/_e9L-qKe2bM`

Table 2: Reaction times for collision detection experiments

Reaction times t_r, in seconds										
0.045	0.055	0.058	0.039	0.052	0.057	0.039	0.029	0.105	0.036	0.060

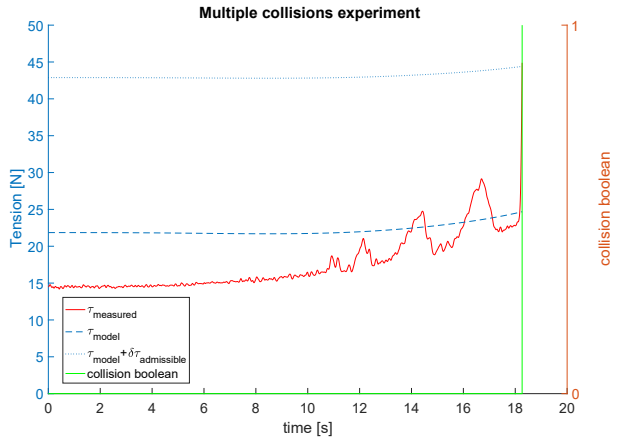

(a) Evolution of the tensions in the cable 1 during a circular translation with multiple short collisions.

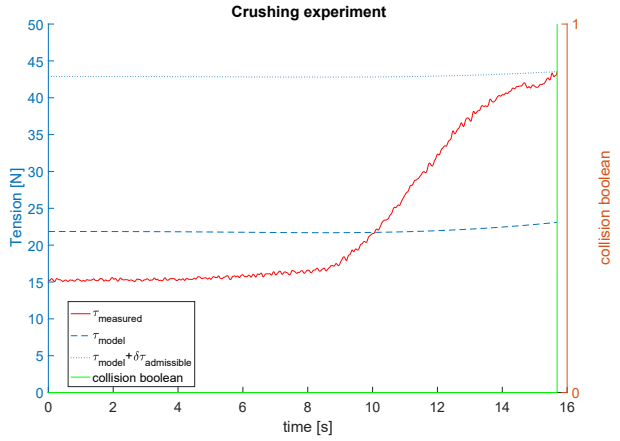

(b) Evolution of the tensions in the cable 1 during a circular translation with a prolonged collision, *i.e.* a crushing situation.

Figure 20: Evolution of the tensions (measured, estimated, admissible) in cable 1 for a trajectory

6. Safe release of the cable

Once a collision between a cable and the environment is detected, the robot may need to act accordingly in order to avoid causing damage. When a cable collides with an operator and remains in tension, it may be crushing their limbs. In that case, it is necessary to design a control strategy allowing the release of the cable, while maintaining the stability of the platform. There are two cases in that event : if the platform is inside the Restrained Static Feasible Workspace - a space defined in 6.1 - a static equilibrium can be found on the same pose. If it is outside, a safe trajectory must be found to reach safely a new equilibrium pose inside the Restrained Static Feasible Workspace without harming the operator on the way while releasing the tension. The latter case is not developed here but will be explored in future work.

6.1. Restrained Static Feasible Workspace

The Static Feasible Workspace (SFW) is the set of all robot poses such that there exists a feasible cable tension vector τ in the tension space τ such that the robot is able to balance the exterior forces wrench $\mathbf{w}_{ext}$, satisfying the equation $\mathbf{W}\tau + \mathbf{w}_{ext} = \mathbf{0}_6$ with $\mathbf{w}_{ext} = \mathbf{w}_g$, $\mathbf{w}_g$ being the gravity wrench [32].

When a cable is no longer applying a tension on the system, either because it is broken, or because it is slack, the effective Static Feasible Workspace is reduced [14]. The resulting workspace can be named Restrained Static Feasible Workspace.

The workspaces calculated before and after zeroing the tension in cable 1 were computed and plotted using MATLAB© with the parameters of the robot prototype, including the coordinates of the end points and the anchor points. The calculated workspaces are displayed in Fig. 21. The first picture shows the SFW before cable 1 (in red) becomes slack, and the second one shows the SFW after setting the maximum tension on cable 1 to 0 N, which is defined as the RSFW, since this cable is now completely slack and exerts no force on the platform.

Only half of the nominal SFW remains accessible once a cable is no longer taut. Hence, any strategy consisting in releasing a cable for safety purposes needs to take into account which area the platform is in, in order to guarantee its equilibrium and preventing an accident.

6.2. Releasing the collided cable in the RSFW

When releasing a cable, the tension needs to be redistributed between the other cables so as to guarantee the static equilibrium of the platform. In this workspace, a feasible solution can always be found regardless of the minimum tension to reach of the collided cable. This problem can still be solved using

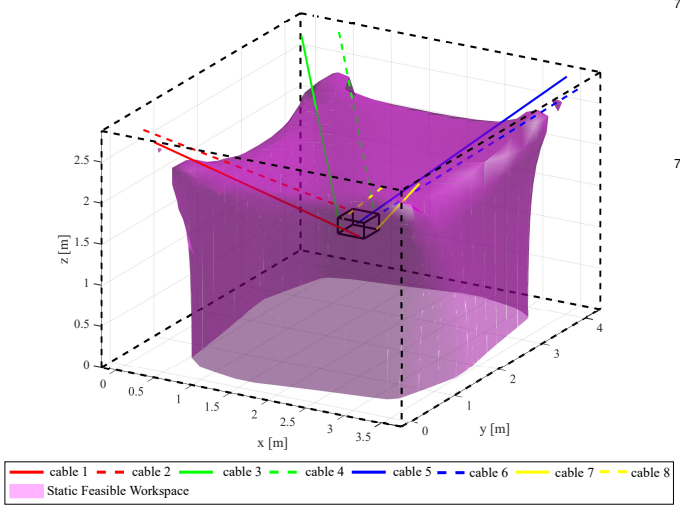

(a) Static Feasible Workspace

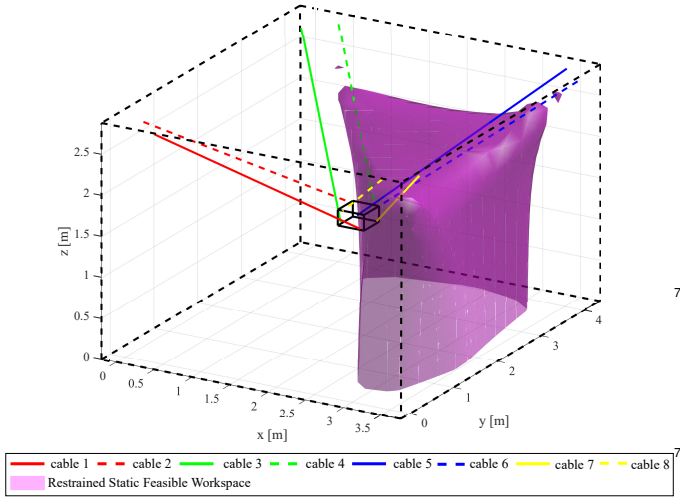

(b) Restrained Static Feasible Workspace, cable tension $\tau_1 = 0$

Figure 21: Static Workspaces of the CDPR

Eq. (18). In that case, the constraints for the minimization criteria change slightly : the maximal tension τ_{max} inside the collided cable will decrease until it reaches the minimal tension (here 0 N) while the maximal tension bound will not be altered for the other cables.

The control scheme modified to take into account the cable collision detection and cable release is presented Fig. 22, with in black the blocks corresponding to the nominal operating mode, identical to Fig. 13, and in red the blocks managing the collision detection and the cable release.

The Threshold block performs a simple collision detection algorithm based on the model established Eq. 11. The pseudo-code of this algorithm is shown in Alg. 1. It returns both the collided cable vector of booleans v_{col}, signaling which on which cable a collision has been detected, and the collision time t_{col}. While this algorithm is able to detect collisions on multiple cables, the cable release strategy proposed in this section applies in the event of a single collision between a cable and the environment.

Algorithm 1 Threshold block algorithm

$t_{col} \leftarrow -1$
$v_{col} \leftarrow 0_m$
while 1 **do**
  $i \leftarrow 1$
  $\tau_{adm} \leftarrow \tau_{ff} + \delta_{\tau R}(\tau_{ff}, f_C^{adm})$
  while $i < m$ **do**
    if $\tau_{m,i} > \tau_{adm,i}$ **then**
      $v_{col}[i] \leftarrow 1$
      $t_{col} \leftarrow t_{clk}$
      return v_{col}, t_{col}
    end if
    $i \leftarrow i + 1$
  end while
end while

A function named $s(t)$ is defined, returning the evolution in proportion of the maximal tension on the collided cable over the post-collision time $t = t_{clk} - t_{col} > 0$. This function is null while no collision is detected and progressively increases to reach 1 after a collision occurred ($t_{col} > 0$). This function then keeps returning 1 the duration needed for the cable to be cleared from the obstacle it met, before decreasing progressively to return the robot to the nominal operating mode. A trapezoidal profile was chosen for the simulations, but sigmoids or other types of functions with a similar profile can be used as well. This function defines the release speed and the release time. These parameters can be set so that the total time between the collision and the end of the release remains under the duration separating the collision and crushing cases[8].

A cable selector **SI** is hence introduced in order to separate the control for the collided and correctly operating cables. It is also necessary to remove the computed torque $\mathbf{\Gamma}_c$ for the collided cable in order to allow its release. Hence the selector is also applied at the output of the corrector block.

[8] Defined to 500 ms in ISO/TS 15066

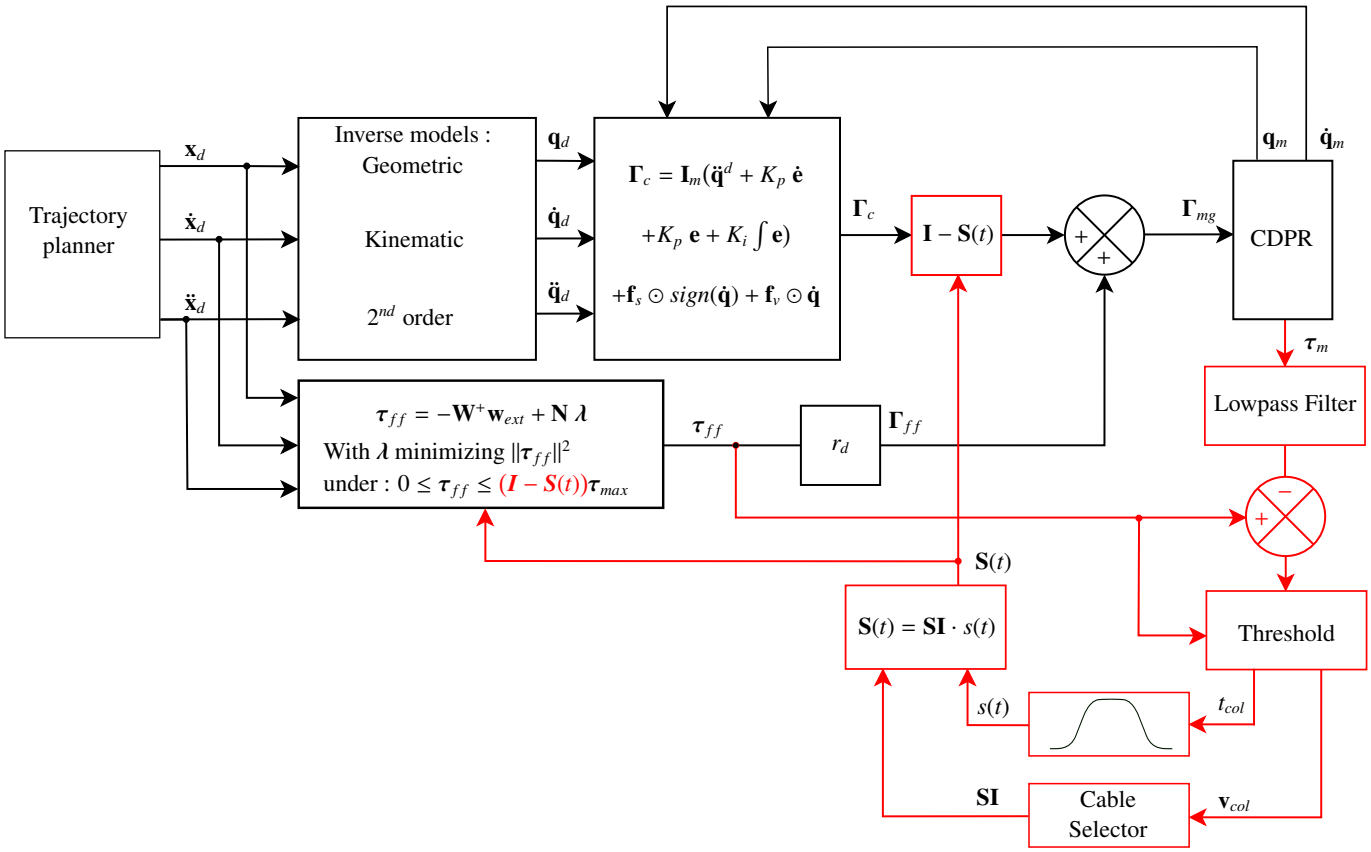

Figure 22: Control scheme for tension redistribution after a collision has been detected

In case of collision detected on a cable i, while the actual tension inside this cable τ_i is significantly higher than the tension predicted by the feedforward term, the tension redistribution of the feedforward torque $\Gamma_{ff,i}$ and the progressive zeroing of the corrector torque $\Gamma_{c,i}$ with the $s(t)$ function result in a null torque for the motor of the collided cable and hence, a null controlled tension inside this cable. Some tension will remain because of the internal friction of the transmission chain, but it should be low enough to easily remove the cable from the obstacles.

A simulation was performed in the static case, where the robot is maintained at a pose $p = [2.5, 3, 0.5, 0, 0, 0]$, inside the RSFW, to observe the redistribution of $\boldsymbol{\tau}_{ff}$ terms. Figure 23 shows the evolution of the predicted cable tensions over time (discretized in equal timesteps), after a collision between cable 1 and the environment has been detected and when the cable release starts. Since only the upper tension bound $\tau_{max,1}$ is controlled by the cable release system, tension distribution remains unchanged while the cable tension $\tau_1 < \tau_{max,1}(t)$. It can be noticed that the cables whose tensions increase are located at the neighboring corners of the main frame, while the tension inside the cables in front of the collided one decreases as well.

The three timestamps, t_1, t_2, t_3, correspond to the three subfigures presented Fig. 24.

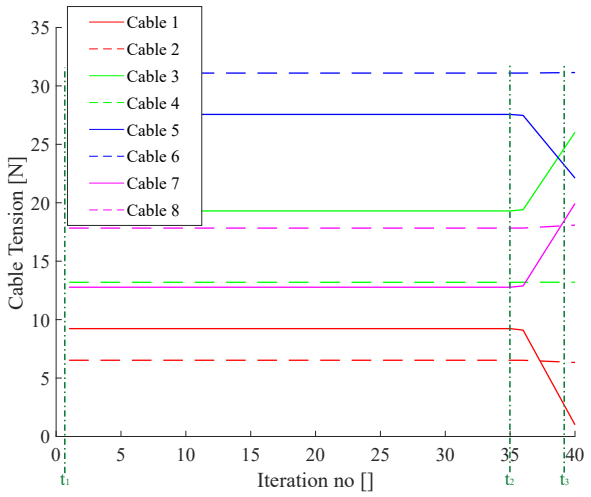

Figure 23: Evolution of the cable tensions during a cable release after a collision in the RSFW

6.3. Feasibility polygon

Varying the upper tension bound τ_{max} for the collided cable to release it consists in effectively translating an edge of the hypercube of feasible tensions $\mathbf{\Omega} = \{\boldsymbol{\tau}_{ff} | \tau_{min,i} \leq \tau_i \leq \tau_{max,i},\ i = [1..m]\}$. All the constraints can be projected into the space of solutions generated by all the sets of $\boldsymbol{\lambda}$. In this study, this is a two-dimensional space Σ where all the constraints are straight lines. The intersection between the feasible tensions hypercube and the space of solutions $\mathbf{\Omega} \cap \mathbf{\Sigma}$ forms the feasibility polygon [33], shown for three different values of $\tau_{max,1}$ Fig. 24.

In these figures, the constraints are represented by straight lines projected into the λ-space of solutions. Cable constraints are paired by color, in full the upper bound and in dotted line the lower tension bound. The feasible polygon is represented by the green surface constrained between the lines, and the chosen solution minimizing the tension squared norm $\|\boldsymbol{\tau}_{ff}\|^2$ is plotted with the blue dot. These figures are plotted at several timesteps, to visualize the evolution of this polygon during the cable release[9].

During the simulation, the line corresponding to the upper tension bound for cable 1 translates towards the line corresponding to the lower tension bound. When the cable is completely released, the system effectively loses a degree of actuation redundancy and solutions are then contained in a 1D space, on a line segment in the 2D space Σ.

7. Conclusion

This paper aimed at establishing a simple but effective model able to detect dangerous collisions between the environment (including operators) and the cables of a suspended CDPR. Besides, a strategy allowing to release the cable tension once a collision has occurred was introduced in order to avoid any prolonged crushing.

A geometric model of the cable deformation under a collision with an external obstacle was introduced and derived to obtain a danger threshold function, returning the admissible cable tension increase in the event of collisions. This function only requires the knowledge of the current cable tension and the admissible force levels to avoid harming operators, without any dependency on the cable length. This model was validated experimentally with an ad-hoc test bench and the collision detection was implemented on the 8-cable suspended CDPR CRAFT prototype, using cable tension sensors and an adaptive control scheme. To detect collisions, the cable tensions measured by the sensors are compared in real time with the admissible cable tension increases.

Then, a strategy aiming at safely releasing a collided and over-taut cable was proposed, along with a control scheme synthesized to perform this task by redistributing the tension in the other cables so as to maintain the moving-platform of the CDPR at a given pose. A strategy to manage the transition between the nominal working mode and the post-collision mode was investigated too. The proposed cable tension management was simulated. The feasibility domain of this tension management, named RSFW, was established and the variation of the tension distribution with time after a collision was detected was simulated.

Future work will deal with the experimental validation of the proposed cable tension management once a cable/human operator collision type occurs while keeping the moving-platform of the CDPR as close as possible to its desired pose. The proposed method could be also be investigated in the case of a tension decrease, resulting for instance from a pulling of the cable towards the tension sensor. Furthermore, recovery strategies for a safe cable release outside the RSFW will be investigated. Beyond simply stopping the robot, other approaches such as a partial cable release or solutions designed for post-cable failure recovery could be used [34, 35, 36]. The implementation and improvement of such methods, ensuring safety of the operators in the whole workspace without stopping the robot and reinitialize it manually, are important steps towards the use of collaborative CDPRs in the industry.

[9] An animated plot was made to observe the evolution of the upper tension bound, the feasibility polygon as well as the chosen solution over time. It can be found here : `https://youtu.be/OZOoVf2KIkM`

Acknowledgments

This work was supported by both the ANR CRAFT project, grant ANR-18-CE10-0004, `https://anr.fr/Project-ANR-18-CE10-0004`, and the European COVR ROCABLE project, COVR Grant agreement ID: 779966 Funded under H2020-EU.2.1.1. Assistance provided by M. Marceau Métillon through the experiments is highly appreciated.

References

[1] S. El Zaatari, M. Marei, W. Li, Z. Usman, Cobot programming for collaborative industrial tasks: An overview, Robotics and Autonomous Systems 116 (2019) 162–180. doi:https://doi.org/10.1016/j.robot.2019.03.003.

[2] P. Long, C. Christine, D. Chablat, A. Girin, An industrial security system for human-robot coexistence, Industrial Robot: An International Journal 45 (12 2017). doi:10.1108/IR-09-2017-0165.

[3] I. El Makrini, K. Merckaert, D. Lefeber, B. Vanderborght, Design of a collaborative architecture for human-robot assembly tasks, in: 2017 IEEE/RSJ International Conference on Intelligent Robots and Systems (IROS), IEEE, 2017, pp. 1624–1629.

[4] J. Krüger, T. K. Lien, A. Verl, Cooperation of human and machines in assembly lines, CIRP annals 58 (2) (2009) 628–646.

[5] R. Meziane, M. J.-D. Otis, H. Ezzaidi, Human-robot collaboration while sharing production activities in dynamic environment: Spader system, Robotics and Computer-Integrated Manufacturing 48 (2017) 243–253.

[6] Z. Bi, C. Luo, Z. Miao, B. Zhang, W. Zhang, L. Wang, Safety assurance mechanisms of collaborative robotic systems in manufacturing, Robotics and Computer-Integrated Manufacturing 67 (2021) 102022.

[7] A. De Luca, A. Albu-Schaffer, S. Haddadin, G. Hirzinger, Collision detection and safe reaction with the dlr-iii lightweight manipulator arm, in: 2006 IEEE/RSJ International Conference on Intelligent Robots and Systems, 2006, pp. 1623–1630. doi:10.1109/IROS.2006.282053.

[8] S. Haddadin, A. De Luca, A. Albu-Schäffer, Robot collisions: A survey on detection, isolation, and identification, IEEE Transactions on Robotics 33 (6) (2017) 1292–1312. doi:10.1109/TRO.2017.2723903.

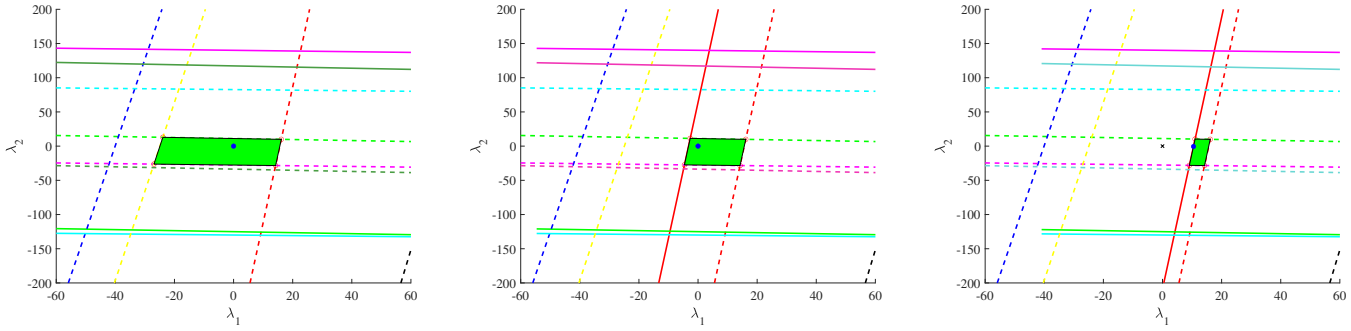

(a) Feasibility polygon at iteration t_1.

(b) Feasibility polygon at iteration t_2

(c) Feasibility polygon at iteration t_3

Figure 24: Feasibility polygons in the λ-space of tension distribution solutions: (*i*) the feasible polygons as a function of the current cable tension limits are shown in green; (*ii*) the blue dot corrresponds to the selected cable tension vector; (*iii*) the red solid straight line corresponds the upper bound t_{1max} of cable 1 tension ((a) $\tau_{max,1} = 80N$, (b) $\tau_{max,1} = 9N$, (c) $\tau_{max,1} = 3N$).

[9] Y. Sugahara, G. Chen, N. Atsumi, D. Matsuura, Y. Takeda, R. Mizutani, R. Katamura, A suspended cable-driven parallel robot for human-cooperative object transportation, in: ROMANSY 23 - Robot Design, Dynamics and Control, Springer International Publishing, Cham, 2021, pp. 109–117. doi:10.1007/978-3-030-58380-4_14.

[10] A. Pott, Cable-Driven Parallel Robots, 1st Edition, Springer, 2018.

[11] N. G. Dagalakis, J. S. Albus, B.-L. Wang, J. Unger, J. D. Lee, Stiffness Study of a Parallel Link Robot Crane for Shipbuilding Applications, Journal of Offshore Mechanics and Arctic Engineering 111 (3) (1989) 183–193. doi:10.1115/1.3257146.

[12] Z. Zhang, Z. Shao, L. Wang, A. J. Shih, Optimal design of a high-speed pick-and-place cable-driven parallel robot, in: Cable-Driven Parallel Robots, Springer International Publishing, Cham, 2018, pp. 340–352. doi:10.1007/978-3-319-61431-1_29.

[13] J.-B. Izard, A. Dubor, P.-E. Herve, E. Cabay, D. Culla, M. Rodriguez, M. Barrado, Large-scale 3d printing with cable-driven parallel robots, Construction Robotics 1 (2017) 1–8. doi:10.1007/s41693-017-0008-0.

[14] S. Caro, J.-P. Merlet, Failure analysis of a collaborative 4-1 cable-driven parallel robot, in: European Conference on Mechanism Science (EuCoMeS 2020): New Trends in Mechanismand Machine Science,, no. 89, 2020, pp. 440–447.

[15] J.-P. Merlet, Analysis of the influence of wire interference on the workspace of wire robot, 2004.

[16] S. Perreault, P. Cardou, C. M. Gosselin, M. J.-D. Otis, Geometric Determination of the Interference-Free Constant-Orientation Workspace of Parallel Cable-Driven Mechanisms, Journal of Mechanisms and Robotics 2 (3), 031016 (07 2010). doi:https://doi.org/10.1115/1.4001780.

[17] A. L. C. Ruiz, S. Caro, P. Cardou, F. Guay, Arachnis: Analysis of robots actuated by cables with handy and neat interface software, in: A. Pott, T. Bruckmann (Eds.), Cable-Driven Parallel Robots, Springer International Publishing, Cham, 2015, pp. 293–305.

[18] D. Bury, J.-B. Izard, M. Gouttefarde, F. Lamiraux, Continuous collision detection for a robotic arm mounted on a cable-driven parallel robot, in: 2019 IEEE/RSJ International Conference on Intelligent Robots and Systems (IROS), IEEE, 2019, pp. 8097–8102.

[19] L. Gagliardini, S. Caro, M. Gouttefarde, A. Girin, Discrete reconfiguration planning for Cable-Driven Parallel Robots, Mechanism and Machine Theory 100 (2016) 313–337. doi:10.1016/j.mechmachtheory.2016.02.014.

[20] U. A. Mishra, S. Caro, M. Gouttefarde, Optimizing Cable-Routing for Reconfigurable Cable-Driven Parallel Robots, in: 5th IEEE/IFToMM International Conference on Reconfigurable Mechanisms and Robots (ReMAR 2021), 2021.
URL https://hal.archives-ouvertes.fr/hal-03338563

[21] J.-H. Bak, S. Hwang, J. Yoon, J. Park, J.-O. Park, Collision-free path planning of cable-driven parallel robots in cluttered environments, Intelligent Service Robotics 12 (07 2019). doi:10.1007/s11370-019-00278-7.

[22] U. A. Mishra, M. Métillon, S. Caro, Kinematic Stability based AFG-RRT* Path Planning for Cable-Driven Parallel Robots, in: The 2021 IEEE International Conference on Robotics and Automation (ICRA 2021), Xi'an, China, 2021.
URL https://hal.archives-ouvertes.fr/hal-03182298

[23] R. Meziane, P. Cardou, M. J.-D. Otis, Cable interference control in physical interaction for cable-driven parallel mechanisms, Mechanism and Machine Theory 132 (2019) 30–47. doi:https://doi.org/10.1016/j.mechmachtheory.2018.10.002.

[24] ISO, Iso/ts 15066:2016 (February 2016).

[25] P. Latteur, Calculer une structure, 3rd Edition, Academia Editions, 2006.

[26] Z. Zhu, S. Meguid, Nonlinear fe-based investigation of flexural damping of slacking wire cables, International Journal of Solids and Structures 44 (16) (2007) 5122–5132. doi:https://doi.org/10.1016/j.ijsolstr.2006.12.024.

[27] D. Gueners, Conception d'un robot parallele a cables pour la fabrication additive, Ph.D. thesis, School of Engineering Sciences, University of Clermont Auvergne, Clermont-Ferrand, France (2021).

[28] L. Mikelsons, T. Bruckmann, M. Hiller, D. Schramm, A real-time capable force calculation algorithm for redundant tendon-based parallel manipulators, in: 2008 IEEE International Conference on Robotics and Automation, 2008, pp. 3869–3874.

[29] A. Pott, An Improved Force Distribution Algorithm for Over-Constrained Cable-Driven Parallel Robots, Vol. 15, 2014. doi:10.1007/978-94-007-7214-4_16.

[30] E. Picard, F. Plestan, E. Tahoumi, F. Claveau, S. Caro, Control Strategies for a Cable-Driven Parallel Robot with Varying Payload Information, Mechatronics 79 (2021) 102648. doi:10.1016/j.mechatronics.2021.102648.

[31] S. Baklouti, Vibration Analysis and Reduction of Cable-Driven Parallel Robots, Ph.D. thesis, INSA de Rennes (Dec. 2018).
URL https://tel.archives-ouvertes.fr/tel-02163227

[32] Z. Zake, Design and stability analysis of visual servoing on cable-driven parallel robots for accuracy improvement, Ph.D. thesis, UMR 6004, Laboratoire des Sciences du Numérique de Nantes, Nantes, France (2020).

[33] E. Picard, S. Caro, F. Plestan, F. Claveau, Stiffness Oriented Tension Distribution Algorithm for Cable-Driven Parallel Robots, in: In : Lenarcic J., Siciliano B. (eds) Advances in Robot Kinematics 2020. ARK 2020. Springer Proceedings in Advanced Robotics, Vol. 15, 2020, pp. 209–217. doi:10.1007/978-3-030-50975-0_26.

[34] A. Berti, M. Gouttefarde, M. Carricato, Dynamic recovery of cable-suspended parallel robots after a cable failure, in: Advances in Robot Kinematics 2016 (ARK2016), Vol. 4, Springer International Publishing, 2018, pp. 331–339.

[35] R. Boumann, T. Bruckmann, Development of emergency strategies for cable-driven parallel robots after a cable break, in: Cable-Driven Parallel Robots, Springer International Publishing, 2019, pp. 268–280.

[36] R. Boumann, T. Bruckmann, Simulation and model-based verification of an emergency strategy for cable failure in cable robots, Actuators 11 (2) (2022). doi:10.3390/act11020056.
URL https://www.mdpi.com/2076-0825/11/2/56

Appendix A. Cable lateral displacement

The derivation of Equation (8) proposed in [25] is described in this Appendix. The model is represented in Fig. 3.

In the case of a static or quasi-static contact (assumption made in this study), the equilibrium of forces applied on the cable at its middle point is expressed by :

$$2(\tau + \delta\tau)\sin\alpha = f_c \tag{A.1}$$

The lateral force f_c induces an increase in tension inside the cable, noted $\delta\tau$ corresponding to an elongation δl. The collision induces an angle α with the initial position of the cable.

$$\delta l = \frac{\delta\tau\, l}{ES} \tag{A.2}$$

From the geometry of the cable deformation model, $\sin\alpha$ can be expressed as :

$$\sin\alpha = \frac{\delta c}{\frac{1}{2}(l + \delta l)} = 2\frac{\delta c}{l}\frac{1}{\left(1 + \frac{\delta\tau}{ES}\right)} \tag{A.3}$$

Then, by combining Eq. (A.1) and Eq. (A.3) :

$$f_c = 4(\tau + \delta\tau)\frac{\delta c}{l}\frac{1}{\left(1 + \frac{\delta\tau}{ES}\right)} \tag{A.4}$$

Then, to simplify this equation, another geometric relationship can be established, using the right-angled triangle and the middle contact properties :

$$\sqrt{\delta c^2 + \frac{l^2}{4}} = \frac{1}{2}(l + \delta l) \tag{A.5}$$

By taking the square of Eq. (A.5) and assuming δ_l^2 is negligible with respect to δ_l, we obtain:

$$\frac{\delta l}{l} = 2\left(\frac{\delta c}{l}\right)^2 \tag{A.6}$$

Then, it is possible to simplify Eq. (A.4) by substituting δl[10] since, from Eqs. (A.2) and (A.6) we have:

$$\frac{\delta\tau}{ES} = 2\left(\frac{\delta c}{l}\right)^2 \tag{A.7}$$

Finally, assuming that $2\left(\frac{\delta c}{l}\right)^2 << 1$:

$$8\left(\frac{\delta c}{l}\right)^3 + 4\frac{\tau}{ES}\left(\frac{\delta c}{l}\right) = \frac{f_c}{ES} \tag{A.8}$$

when using the normalized values, Eq.(A.8) amounts to Eq. (8).

[10] It would also be possible to replace δc since we are looking for δl leading to $\delta\tau$ but it also leads to an equivalent cubic problem, providing no advantage on using directly the formula provided in [27].